Sex-specific thermoregulatory effects of estrogen signaling in *Reprimo* lineage cells

Authors:
Jae W. Park[1*], Laura R. Cortes[1*#], Norma P. Sandoval[1], Alejandra G. Baron[1], Adriana R. Vree[1], Higor J. Fideles[1], Mia R. Hansen[1], Julissa I. Lopez[1,2], Elizabeth A. Dilday[1], Sakina Rashid[1], Laura G. Kammel[1], J. Edward van Veen[1], Stephanie M. Correa[1#]

Affiliation:
[1]Department of Integrative Biology and Physiology, University of California, Los Angeles, California, USA
[2] Cypress College, Cypress, CA, USA

*co-first authors
[#]authors for correspondence: lauracortes@ucla.edu and stephaniecorrea@ucla.edu

The authors have nothing to disclose.

Abstract

Menopause affects over a million individuals annually and is characterized by variable and declining ovarian hormones. Decreasing estrogen levels impact energy homeostasis and increases the risk of metabolic disorders. Energy expenditure is largely directed towards thermoregulation, which is modulated in part by estrogen receptor (ER) α expressing neurons in the hypothalamus. Whether specific sub-populations of ERα+ neurons control the effects of estrogens on thermogenesis remains poorly understood. This study investigates the function of ERα in neurons that express *Rprm* (Reprimo), a gene we previously linked to thermoregulation in females. Here, we use a novel *ReprimoCre* mouse to selectively knock out ERα in *Rprm* lineage neurons (Reprimo-specific estrogen receptor α KO; RERKO) and report changes in core temperature in female mice, with no changes in body weight, body composition, or food intake. RERKO females have elevated brown adipose tissue (BAT) temperature and lower tail temperature relative to controls, suggesting increased heat production and impaired heat dissipation, respectively. Developmental expression of *Rprm* was detected in the brain, but not in BAT or white adipose tissue suggesting temperature changes may be mediated by the nervous system. Thus, we next ablated *Rprm* expressing neurons in the ventrolateral area of the ventromedial nucleus of the hypothalamus (VMHvl) and observed a reduction in core temperature and increased fat mass in ablated female mice relative to controls. Taken together, these results show that estrogen signaling in *Rprm* expressing cells and VMHvl^{Rprm} neurons are critical for thermoregulation, mainly through the modulation of brown adipose tissue thermogenesis in female, but not male mice.

Keywords: Estrogen receptor alpha, thermogenesis**,** energy expenditure, *Reprimo*, metabolism, ventromedial nucleus of the hypothalamus

Introduction

Over a million people transition into menopause each year, with a majority experiencing side effects that alter their quality of life [1]. Estrogens are potent modulators of energy homeostasis [2–4]. Thus, plummeting levels of estrogen during menopause are associated with dysregulation of metabolism [5]. Menopausal people experience hot flushes and reduced energy expenditure; the latter contributes to greater adiposity, body weight, and risk of metabolic disorders [6–9]. Energy expenditure is regulated by estrogen-sensitive neurons in the hypothalamus [10–14]. Recent work suggests that distinct groups of hypothalamic estrogen receptor (ER) α + may regulate specific aspects of energy homeostasis [11,12,14]. Pinpointing these neural subsets and their precise functions can lead to a mechanistic understanding of energy expenditure and inform cell-based therapeutics tailored to specific symptoms in menopausal and obese patients.

Rodents are suitable models to study the hormonal regulation of energy expenditure. Like menopausal people, mice lacking ovaries have lower energy expenditure and increased body weight and adiposity [15], and estradiol administration blunts these changes [16]. Although ERα (*Esr1*) is found throughout the body, its expression in the central nervous system (CNS) is necessary for energy homeostasis. Mice with *Esr1* knocked out (KO) in the nervous system have greater body mass, and specifically, females consume more food and have reduced energy expenditure relative to controls [10]. The neural circuitry involved in energy homeostasis includes the ventrolateral area of the ventromedial nucleus (VMHvl), the medial preoptic area (MPO), and the arcuate nucleus (ARH). These hypothalamic regions contain abundant expression of ERα. Female mice and rats with *Esr1* knockdown in the VMHvl have lower activity levels, basal metabolic rate, and energy expenditure as assessed via indirect calorimetry, resulting in higher body weight relative to controls [17,18]. Similarly, female mice with *Esr1* KO in the VMHvl have lower metabolic rates and thermogenesis [10]. Conversely, activating *Esr1*+ VMHvl (VMHvl^{Esr1}) neurons increases heat production and movement [12]. Thus, the VMHvl is essential for the regulation of energy expenditure. In contrast, the effects of estrogens on food intake are regulated by other regions, including the nearby ARH. Knocking out *Esr1* in POMC+ cells increases food intake and body weight in females relative to controls [10]. Similarly, silencing steroid and metabolic hormone-responsive ERα/Kisspeptin+ neurons in the ARH causes obesity in female mice and alters circadian feeding patterns [19–22]. Lastly, activation of

MPO^{Esr1} cells leads to a hypometabolic state akin to torpor; temperature, energy expenditure, metabolic rate, and movement plummet [13]. In summary, VMHvl^{Esr1} cells promote energy use, *Esr1* in ARH cells alters food intake, and MPO^{Esr1} cells trigger a profound energy conservation state.

Intermingled within the same nuclei, ERα+ cells may differ in their function, connections, and neurochemical identity (*i.e.*, their gene expression pattern) [23,24,12,25]. For example, a study using preoptic area slices from rats showed that a portion of estrogen-responsive MPO neurons (likely expressing ERα) are temperature-responsive, with some responding to warmth and others to cold [26]. In a similar fashion, VMHvl^{Esr1} cells differ in their response to glucose and neural connectivity [27,25]. About half are excited by an increase in glucose levels and project to the dorsal raphe nucleus, whereas the other half are excited by a depletion of glucose levels and project to the arcuate nucleus [25]. Functional specialization among ERα+ cells suggest that they may differ in the expression of peptides and proteins that shape their roles and responses. Indeed, our lab found that VMHvl^{Esr1} cells are neurochemically distinct. Using single-cell sequencing, we found sub-populations of VMHvl^{Esr1} neurons marked by the expression of substance P (Tachykinin 1; *Tac1*), reprimo (*Rprm*), or prodynorphin (*Pdyn*). Intriguingly, females have many more ERα neurons that express *Tac1* and *Rprm*, and manipulating these cells differentially alters energy expenditure. Mice that are missing a subset of VMHvl^{Esr1} cells that co-express *Tac1* and *Nkx2-1* or have inactivation of the *Mc4r* subpopulation move less [11,14]. With *Tac1/Nkx2-1* cell loss, this also leads to increased adiposity and body weight [11]. Interestingly, *Rprm* knockdown in the VMHvl leaves movement intact, but increases core temperature and thermogenesis. These findings suggest specialization of cell populations or gene function within the VMHvl.

The function of *Rprm*, a tumor suppressor gene, and *Rprm*+ neurons has been largely unexplored outside of pathological contexts [28–30], with the exception of this study [31]. In the present work, we test the function of *Rprm*+ cells on energy expenditure. Specifically, we hypothesize that *Esr1* expression in *Rprm*+ cells is necessary for the modulation of body temperature via thermogenic brown adipose tissue (BAT) [32]. We generated a mouse that expresses Cre recombinase under the control of *Rprm* to selectively knock out *Esr1* in *Rprm* lineage cells. Despite the extensive effects of global and CNS-specific *Esr1* knockout on weight, food intake and movement [10,33,34], *Esr1* KO in *Rprm* lineage cells produces a more restricted

phenotype. Core temperature is altered between controls and KO, while body weight, body composition, and food intake are largely unaffected. Furthermore, BAT mass is heavier and produces more heat, indicating increased thermogenesis. Because *Esr1* and *Rprm* were co-expressed in several brain areas and parts of the body, we next ablated *Rprm* cells in the VMHvl to test their specific role in modulating temperature. Core temperature was decreased in ablated mice relative to controls, and BAT mass was increased while movement was unaffected. In summary, our data suggest that *Esr1* in *Rprm* lineage cells and VMHvl^{Rprm} neurons specifically modulate core temperature, while leaving other aspects of energy expenditure intact.

Methods

Generation of Rprm^{Cre} knock-in mice

The donor construct consisted of a double stranded DNA repair cassette that included the coding sequence for *Rprm* linked to the codon-improved cre recombinase (*iCre*) sequence via a P2A peptide. The P2A peptide leads to ribosomal skipping and the generation of distinct peptide products, in roughly equal amounts, from a single multi-cistronic construct (Kim et al 2011). A 21-bp nuclear localization sequence (NLS) is located at the 5' end of the *iCre* exon and helps direct proteins into the nucleus. To induce proper DNA insertion, we also included homology arms (approximately 2,000 bp) both upstream and downstream of the *Rprm* and *iCre* coding sequences. Finally, 34-bp long flippase recognition target (FRT) sites were inserted in the upstream and downstream homology arms within 250 bp of the 5' and 3' exons. The total length of the construct is approximately 8.3 Kb.

Esr1$^{f/f}$ female mice [35] were paired with *Rprm*^{Cre};*Esr1*$^{f/f}$ studs to generate **R**eprimo-specific **E**strogen **R**eceptor α **K**nock **O**ut (RERKO) on a mixed B6;129P background. In other words, RERKO mice had *Esr1* knocked out (KO) in *Rprm* lineage cells. Mice were bred and maintained in approved conditions at the University of California Los Angeles. Control littermates were *Esr1*$^{f/f}$ and denoted WT for the *Rprm*^{Cre} mutation. For lineage experiments, *Rprm*^{Cre} mice on a C57BL/6J background were paired with *Ai14*$^{f/f}$ reporter mice (Jax #007914; Madisen et al., 2010) to generate offspring that fluoresce tdTomato in tissues expressing *Rprm* (*Rprm*^{Cre}; *Ai14*$^{f/+}$). Mice were kept in 12:12 light cycle conditions (zeitgeber time (ZT) 0 = 7 am) at ~23 °C and ~30% humidity with food and water provided *ad libitum*. All animal studies were approved by the UCLA Institutional Animal Care and Use Committee (IACUC) and were carried out following the recommendations of the Guide for the Care and Use of Laboratory Animals of

the National Institutes of Health.

Surgeries

For all surgeries, mice were anesthetized with isoflurane and administered buprenorphine (0.01 mg/mL) and carprofen (0.58 mg/mL) on the day of surgery and the following day to manage pain and inflammation.

Probe implants

G2 eMitters (Starr Life Sciences; Oakmont, PA, USA) were placed into the abdominal cavity to record core temperature and locomotion. Cubisens TS100/TS110 probes (Cubeworks; Ann Arbor, MI, USA) or Nano-T loggers (Star-Oddi, Garðabær, Iceland) were secured subcutaneously above the BAT depots and over the base of the tail to gauge heat generation and dissipation, respectively. Custom sleeves were designed to secure probes above BAT and tail using Autodesk Fusion 360 (San Francisco, CA, USA) and UltiMakerCura software (New York, NY, USA). Sleeves were printed on a Creality Ender-2 V2 3D printer using PLA filament. Files are publicly available on NIH 3D (Reference model: 3DPX-020322; https://3d.nih.gov/entries/3DPX-020322).

Stereotaxic surgery

Control (*pAAV8-Syn-FLEX-Mac-GFP*) or caspase virus (*pAAV2-flex-taCasp3-TEVp*) was delivered into the VMHvl (AP 1.58, ML ± 0.65, DV 5.7) in 8-week-old C57Bl6J wildtype or *RprmCre* mice [36,37]. Each hemisphere received 100 nL at 5-10 nL/sec using a 10 µL Hamilton syringe attached to a pulled glass needle. Mice recovered for two weeks before starting three days of temperature and locomotion recordings which were averaged hourly.

Collection

Mice were perfused with 4% paraformaldehyde (PFA; Electron Microscopy Sciences; Hatfield, PA, USA) in 0.01M phosphate-buffered saline (1x PBS). Brains were stored in 4% PFA overnight at 4°C and transferred to 30% sucrose in 1x PBS until brains sank. Brains were embedded in Optimal Cutting Temperature compound (OCT; Fisher Scientific, Fair Lawn, NJ, USA) and stored at -80°C until cutting. BAT, inguinal white adipose tissue (iWAT), and gonadal white adipose tissue (gWAT) were dissected and stored in tissue cassettes submerged in 70% ethanol until staining.

Metabolic and reproductive phenotyping

Mice were group housed according to sex, and body weight was recorded weekly from 5 to 16 weeks of age. A separate cohort of mice were weighed and placed into an EchoMRI^{tm} (Houston, TX, USA) to record fat and lean mass at 16 weeks of age. To record food intake, a pre-measured allotment was provided on day one to singly housed mice. After seven days, the remaining food was subtracted from the weight of food initially provided, and the resulting weight was divided over seven days to provide a daily average of food consumption. To record core temperature and locomotion, mice were placed on ER4000 energizer/receiver pads in their home cages (version 5, VitalView software, Starr Life Sciences). All temperature and activity measurements were collected every five minutes across three to five days. For temperature and activity recordings, an average for each hour of the day (ZT 0 – 23) across recording days was calculated. Raw data from G2 emitters, TS100/TS110 probes, and Nano-T loggers were exported in CSV format using Vitalview (Starr Life Science), TS GUI (Cubeworks), and Mercury (Star-Oddi), respectively. Data was prepared for analysis in Microsoft Excel (Microsoft Corporation; Redmond, Washington, USA). R Studio (R version 4.3.1; Boston, MA, USA) was used to process the data and generate hourly averages (code for processing and plotting provided at https://github.com/kodori00/Rscript). To track the estrous cycle, mice underwent vaginal lavage using 0.9% saline every morning between ZT 1-2.

Histology

Cytology

For estrous cycling, vaginal lavages were deposited onto slides, stained with Giemsa (0.6% in 1x PBS;) to visualize nucleic acid and distinguish cell morphology, and imaged using light microscopy as described in Massa et al., 2023. The estrous stage was determined by the relative amounts of leukocytes and cornified and nucleated epithelia (Byers et al., 2012). BAT and iWAT were sectioned into 4 µm slices and stained with hematoxylin and eosin by the UCLA Translational Pathology Core Laboratory.

Immunohistochemistry

Brains were coronally cryo-sectioned into four or six 20-30 µm series and stored on slides or in cryoprotectant (30% sucrose, 30% ethylene glycol, and 1% polyvinylpyrrolidone in 1x PBS) at -80°C until use. One series of 30 µm thick sections underwent immunohistochemistry to validate the loss of ERα expression in RERKO mice (rabbit anti-ERα, 1:1000, ThermoFisher Invitrogen,

Waltham, MA) and one series of 20 µm sections was used to validate the loss of ERα cells in caspase-treated mice (rabbit anti-ERα, 1:500, Millipore Sigma, Burlington, MA). Tissue was rinsed in 1x PBS and blocked for one hour at room temperature (RT) in either 10% bovine serum albumin (BSA) and 2% Normal Goat Serum (NGS) or 10% NGS in 0.3% PBS-Triton X depending on antibody. After blocking, tissue was incubated in primary antibody overnight at 4°C or RT. The following day, the tissue was incubated with either Alexa Fluor 546 (1:500; ThermoFisher) or 647 (1:1000; Jackson ImmunoResearch Laboratories, West Grove, PA, USA) anti-rabbit secondary antibody for 1.5-2 hours at RT. Nuclei were counterstained with 4′,6-diamidino-2-phenylindole (DAPI, 1:500-1000, ThermoFisher Invitrogen), and Fluoromount-G was used to coverslip (Southernbiotech, Birmingham, AL, USA).

Fluorescent In-Situ Hybridization

Flash-frozen brains containing the MPO and the VMHvl were coronally cryo-sectioned into six series at 16 µm. Tissue underwent single molecule *in-situ* hybridization according to manufacturer instructions in the RNAscope Multiplex Fluorescent Detection Kit version 2 (Advanced Cell Diagnostics, Newark, CA, USA). Tissue was fixed in 4% PFA for 15 minutes and pre-treated using serial ethanol dilutions, hydrogen peroxide, and protease IV solution (incubation time shortened to 7 minutes to prevent tissue degradation). Tissue was incubated with probes targeting *Rprm* and *Esr1* at 40°C for 2 hours. Afterward, the probe signal was amplified and fluorescently labeled with Opal 520 and 690 (Akoya Biosciences, MA, USA) at 1:1000 dilution for *Rprm* and *Esr1*, respectively. Signal was developed using horseradish peroxidase and counterstained with reagents provided in the kit. Slides were cover-slipped using Prolong Gold Antifade (ThermoFisher Scientific).

Imaging & analysis

Brightfield images of BAT and iWAT histological sections were taken by a Leica DM1000 microscope (Leica Microsystems Inc, Deerfield, IL, USA). Brain, uterine and ovarian sections were imaged using a Nikon Eclipse Ti2 inverted microscope. Peripheral tissues were illuminated using a Leica MZ10F and imaged using a dual MP camera system on an iPhone13. ERα cells were counted in the anteroventral periventricular area (AVPV), medial preoptic area (MPO), ventromedial ventrolateral area (VMHvl), and arcuate nucleus (ARH) of the hypothalamus. Regions of interest were determined by examining the shape of the anterior commissure and

median eminence and referencing the Allen Brain Mouse (v2, 2011) and Paxinos and Franklin (v3, 2008) atlases. The machine learning software Ilastik (Berg et al., 2019; www.ilastik.org/about) segmented ERα+ cells from the background. Positive object outlines were loaded to CellProfiler 4.2.5 (Stirling et al., 2021; www.cellprofiler.org), overlaid over the fluorescent images, manually edited if necessary, and counted. Cell counts were averaged across hemispheres; if one hemisphere was damaged, the count on the intact side was used.

Statistics

Statistical analyses and plots were made in Prism (version 10.2.3 for Mac; GraphPad Software, Boston, MA, USA). When applicable, two-way ANOVAs or mixed-effects models were run with repeated (age or ZT) and independent (genotype or sex) factors. Post hoc comparisons between control and RERKO mice at each time point were performed using Šídák's multiple comparisons test. A t-test was used to compare means for analyses only performed in females.

Results

3.1 Developmental *Rprm* expression is detected throughout the brain and periphery

We bred *RprmCre* mice with *Ai14* reporter mice to identify the tissues capable of expressing *Rprm* (Figure 1A), We report Cre-mediated expression of TdTomato in the brain, uterus, ovary, pancreas and pituitary (Figure 1B, C; Supp. Figure 1). ERα (*Esr1*) is also expressed in the uterus, ovary, pancreas, pituitary, and various hypothalamic regions [38,39], thus these tissues are expected to contain the *Rprm*-conditional mutation targeting *Esr1* in RERKO mice. Conversely, TdTomato expression was absent from BAT, iWAT, and gWAT (Figure1C right). To probe further into the areas of the adult brain co-expressing *Esr1* and *Rprm*, we performed single molecule *in situ* hybridization to label *Esr1* and *Rprm* and detected both transcripts in the AVPV, MPO, VMHvl, and ARH (Figure 1D).

3.2 *Esr1* knockout in *Rprm* lineage cells (RERKO) leads to an increase in brown adipose tissue mass, specifically in females

Previous studies report that global ERα knockout or VMHvl-specific ERα knock-down increases body weight, feeding, and fat mass in mice [17,33]. In contrast, we report that body weight in RERKO mice is largely unchanged relative to controls (Supp. Figure 2). Male RERKO mice became subtly heavier than controls as they aged (genotype x age interaction: $F_{11,318} = 2.398$, $p < 0.0001$), and female body mass was unaffected. Instead, we observed a sex-specific effect of

RERKO on BAT mass (genotype x sex interaction: $F_{1,40} = 24.5$, $p < 0.0001$; Figure 2A) and no effect on iWAT (Figure 2B). Female RERKO mice had larger BAT depots than controls ($p < 0.0001$), while BAT size in males did not differ (Figure 2A). BAT tissue in RERKO mice appeared lighter in color and typically had larger adipose droplets relative to controls (Figure 2C, D) – although an analysis comparing nuclei and adiposity in BAT did not reach significance (Supp. Figure 3). In contrast to global *Esr1* KO [17,33], RERKO mice have no changes in adiposity: percent fat mass and body mass as recorded via EchoMRI were similar between RERKO and control littermates (Figure 2E-G). In addition, RERKO mice did not consume more food relative to controls (Figure 2H) as reported in CNS-restricted *Esr1* KO mice [10]. Together, these data suggest that *Esr1* in *Rprm*+ cells may regulate discrete facets of metabolism (*i.e.*, BAT), while sparing energy intake and storage.

3.3 *Esr1* knockout in *Rprm* lineage cells sex-specifically impacts energy expenditure

Because BAT contributes to thermoregulation, we next tested if RERKO mice had changes in body temperature by implanting telemetry probes that simultaneously and passively record core, BAT, and tail temperature (Figure 3A). In males, core temperature and locomotion were unaffected by genotype (Figure 3B, C), consistent with no change in BAT mass. In contrast, both temperature (genotype x ZT: $F_{23,437} = 6.0$, $p < 0.0001$; Figure 3D) and locomotion (ZT x genotype: $F_{23,391} = 1.7$, $p = 0.02$; Figure 3E) differed between WT and RERKO female mice. Probing further, we compared BAT and tail temperature as proxies for heat generation and dissipation, respectively. Female RERKO mice had higher BAT temperature than WT mice (main effect of genotype: $F_{1,14} = 4.7$, $p < 0.05$; Figure 3F) and lower tail temperature than WT mice (main effect of genotype: $F_{1,6} = 8.6$, $p < 0.05$; Figure 3G). Hence, female RERKO mice appear to produce more heat and dissipate less heat, contributing to their altered core temperature phenotype. In line with our morphological findings, ERα in *Rprm*+ cells appears to specifically regulate thermogenesis in a sex-specific manner.

In addition to altered thermogenesis, RERKO female mice appeared to have reproductive deficits. RERKO mice did not cycle well, mostly remaining in diestrus or metestrus (Supp. Figure 4A, B). RERKO mice had heavier ovarian ($t_8 = 2.5$, $p < 0.05$) and uterine masses ($t_{23} = 5.9$, $p < 0.0001$; Supp. Figure 4D), and histological examination revealed abnormal ovarian and uterine anatomy (Supp. Figure 4C). Sex steroid hormones influence thermoregulation [40,41]; thus, it is possible that differing hormonal milieu between WT and RERKO underlie the

temperature phenotype. To address this, females were ovariectomized, and temperature was compared between WT littermates and RERKO mice seven days later. There was a main effect of genotype ($F_{1,12} = 5.5$, $p < 0.05$) and an interaction between genotype and hour of day ($F_{23,270} = 1.7$, $p < 0.05$; Supp. Figure 5). Ovariectomized RERKO mice had elevated temperature relative to ovariectomized controls, particularly during the light phase (Supp. Figure 5). Thus, RERKO mice have altered thermoregulation, that is at least partially, independent from changes in ovarian hormones.

3.4 *Esr1* knockout in *Rprm* cells reduces ERα immunoreactivity in thermoregulatory hypothalamic regions.

In the brain, ERα is expressed in brain regions involved in thermoregulation and energy intake and expenditure (*e.g.*, MPO, VMHvl, and the ARH) [13,42]. Interestingly, *Rprm* is co-expressed in all of these regions (Figure 1D). RERKO mice had fewer ERα cells in the AVPV, VMHvl, and ARH (Figure 4D, F, G). Notably, we did not observe an effect of RERKO on ERα+ cell counts in the MPO, an area containing estrogen sensitive neurons that can drive a torpor-like state (Figure 4E)[13]. We note that the sex difference in ERα in the VMHvl was completely abolished in RERKO mice, due to a reduction in both sexes (Figure 4F). We did not have sufficient power to confirm the expected sex difference in ERα cell counts in the AVPV, but nevertheless, observed a decrease in RERKO mice relative to controls in males and females (Figure 4D).

3.5 Ablating *Rprm*+ cells in the VMHvl decreases core temperature and increases fat depots.

We hypothesized that the temperature phenotype in RERKO mice may involve the VMHvl given our previous work [12]. To test this, we delivered an AAV expressing a Cre-dependent and self-activating caspase into the VMHvl of *RprmCre* mice to specifically ablate *Rprm*+ cells in this brain region [37]. Because there is not an acceptable antibody for Reprimo, we labeled ERα to validate caspase-mediated cell death of *Esr1*/*Rprm* cells in the VMHvl. We observed a decrease in ERα+ immunoreactivity between controls and caspase-treated mice in the VMHvl (Figure 5C), but not in the ARH (Figure 5D). Caspase-treated mice had decreased core temperature (main effect of group: $F_{1,10} = 11.20$, $p < 0.01$; Figure 5E) and heavier BAT ($t_{10} = 4.02$, $p < 0.01$), iWAT ($t_{10} = 2.23$, $p = 0.05$), and gWAT ($t_{12} = 4.03$, $p < 0.01$). Activity levels were unaffected by

caspase treatment (Figure 5F), as was total body mass (Figure 5G) or uterine mass (Figure 5K). This provides additional evidence that *Rprm*+ neurons regulate thermogenesis [12]. Importantly, we observe these effects without an effect on the uterus, a bioassay for circulating estrogen levels [43], suggesting that this effect is not secondary to any potential changes in circulating estrogens.

Discussion

We investigated the role of *Esr1* in *Rprm*+ cells and the specific contribution of VMHvl^{Rprm} neurons on energy homeostasis. First, we characterized the *Rprm* lineage using a novel *RprmCre* mouse and an *Ai14* reporter. We observed *Rprm*-driven tdTomato expression in the pancreas, uterus, ovary, pituitary, and brain. Interestingly, we did not observe the expression of *Rprm* in fat depots associated with heat generation or retention, including BAT, iWAT, or gWAT. Figueroa et al. proposed that *Rprm* expression is conserved given limited, yet similar expression in intestinal, vascular, and neural tissues in both humans and zebrafish [31]. Building on the idea that *Rprm* has limited expression patterns, it is intriguing that *Rprm* appears predominantly expressed in hormone-producing or hormone-transporting tissues (*i.e.*, ovaries, pituitary, pancreas, brain, and blood vessels). In particular, these tissues are estrogen sensitive [44–46]. This pattern suggests that *Rprm* may play a role in hormonal regulation, potentially influencing hormone receptor function in specific tissues or cell-types.

Next, we tested the role of *Esr1* in *Rprm*-expressing cells using *Rprm*^{Cre}; *Esr1*$^{f/f}$ (RERKO) mice. In the adult brain, *Esr1* and *Rprm* are co-expressed in at least four hypothalamic nuclei: the AVPV, the MPO, the VMHvl, and the ARH. RERKO mice had reduced ERα+ cell counts in all of these regions, except the MPO. These regions are associated with energy homeostasis and reproduction prompting us to compare these phenotypes in wildtype and RERKO mice.

As mice aged to four months, there was a subtle increase in body weight in males, but not females. However, there were no significant differences in fat mass, lean mass, or food consumption between RERKO mice and their WT siblings in male or female mice. We observed a reduction in ERα+ cells in the ARH, suggesting that *Rprm*-negative ERα cells in the ARH may instead modulate food intake. The most notable phenotype was a doubling of BAT mass that was specific to females. This was surprising since previous studies on global *Esr1* KO mice report significant weight gain and adiposity, but no change in BAT mass [33,34]. Thus, despite expecting *Esr1* to be knocked out across multiple tissues in the *Rprm* lineage, *Esr1* loss in *Rprm*+ cells resulted in a more restricted phenotype.

Because we found the strongest effect of RERKO on the mass of thermogenic BAT, we compared the temperature of the core, BAT and tail skin. Control mice displayed typical circadian changes in core body temperature with lowered core and BAT temperatures in the inactive phase. Interestingly, core and BAT temperature in the inactive phase was higher in RERKO mice relative to controls, while tail temperature was reduced. The effect on core temperature was observed in females but not males, suggesting that estrogen signaling in the *Rprm* lineage is particularly important for maintaining normal temperatures in females. Moreover, BAT and tail temperature appear to lose circadian rhythmicity, with BAT temperature remaining high during the day in RERKO females. RERKO mice have lower core temperatures in the active phase, contributing to a stabilization of core body temperature across the dark and light cycles. In summary, we posit that without *Esr1* in *Rprm* lineage cells, BAT thermogenesis and tail dissipation lack circadian fluctuations and contribute to a plateauing of core body temperature in RERKO mice.

In addition to differences in thermoregulation, we observed reproductive deficits in female RERKO mice: they did not cycle well and had abnormal reproductive anatomy. Thus, a limitation of this mouse model is potential differences in hormone levels, which may indirectly alter physiology and metabolism. To address this, we ovariectomized RERKO and WT mice and found persistent differences in core temperature. Ovariectomized RERKO mice still had elevated core temperature that was most pronounced in the inactive phase. Notably, temperature did not appear to differ between RERKO and controls in the first half of the active phase. Thus, the decrease in temperature in the active phase may be hormonally-driven rather than a direct consequence of ERα ablation, and thus not apparent in ovariectomized RERKO mice. It is tentatively promising that the increase in temperature in the inactive phase remains in ovariectomized mice, supporting the idea that estrogen regulation in *Rprm* lineage cells may be important for diurnal decreases in temperature.

Because we did not detect developmental *Rprm* expression in BAT nor iWAT, we hypothesized that RERKO mice had altered central regulation of energy expenditure. Movement and BAT-mediated thermogenesis are associated with the VMHvl [11,12], making it the most promising mediator of a temperature phenotype. To conclusively test that *Rprm*/*Esr1* neurons are involved in thermogenesis, we ablated *Rprm*+ cells in the VMHvl by stereotaxic delivery of a Cre-dependent caspase. We observed a ~40% decrease in the number of ERα cells in the

VMHvl, consistent with our prior observation that 41% of ERα cells co-express *Rprm* [12]. Notably, the number of ERα cells in the nearby ARH was not affected. Caspase-treated mice had lower core temperature than controls with no changes in movement, similar to previous effects of knocking down *Rprm* in the same region [12]). We also observed heavier BAT mass in caspase-ablated mice, suggesting an effect on BAT-mediated thermogenesis. Together, these studies suggest that VMHvl^{Rprm} cells increase core body temperature and that the effects of *Esr1* KO in the *Rprm* lineage cells are likely mediated by the VMHvl.

Conclusion

In summary, we use an intersectional gene expression knockout approach to show that estrogen-dependent regulation of *Rprm* cells alters temperature, partly by modulating BAT thermogenesis and heat dissipating processes. *Rprm* expression is not found in brown or white adipose tissue, suggesting *Esr1* in *Rprm* neurons (as opposed to in adipose tissue) is critical for proper thermoregulation. Specifically, it appears that *Rprm*+ cells in the VMHvl drive heat generation via BAT. This adds to a body of literature showing specialization of sub-populations of ERα neurons or gene function in the VMHvl [11,14,23,25,47]. By identifying the cells driving regulation of thermogenesis, our research opens potential avenues for new precision treatments in metabolic disorders, such as obesity and menopause.

Acknowledgements

The authors thank Monay Martinez for assistance with imaging and members of the Correa lab, particularly Paul Vander and Rachel Scott, for their feedback on the manuscript.

Author contributions

SMC, LRC, and JWP conceptualized the present studies. JEV, SMC, and LGK designed the *Rprm-Cre-FRT* mouse, and JWP designed the telemetry probe sleeves. JWP, LRC, NPS, AGB, ARV, HJF, MRH, EAD, and SR contributed to experimental research and data collection. JWP, LRC, ARV, HJF, and JIL provided data analysis and validation. SMC, LRC, and LGK provided funding and/or resources to complete the studies, and SMC provided mentoring and laboratory space. LRC and SMC wrote the manuscript with input from JWP, NPS, and JEV.

Funding Sources

These studies were supported by the National Institute of Aging (R01AG066821) and National Institute of Diabetes and Digestive and Kidney Diseases (NIDDK; R01DK136073) to SMC and by the National Institute of Child Health and Development (K00HD109205), the Burroughs Wellcome Foundation Postdoctoral Enrichment Fellowship, the Iris Cantor-UCLA Women's Health Center Executive Advisory Board (NCATS UCLA Clinical and Translational Science Institute; UL1TR001881), and the NIDDK UCLA LIFT-UP (Leveraging Institutional support for Talented, Underrepresented Physicians and/ or Scientists) - National Institutes of Health Office of Disease Prevention, (ODP; U24DK132746) to LRC. The generation of the *Rprm-Cre-FRT* mouse was funded by a UCLA Brain Research Institute Predoctoral Research Grant to LGK.

References

[1] Peacock, K., Carlson, K., Ketvertis, K.M., Doerr, C., 2024. Menopause (Nursing). StatPearls, Treasure Island (FL): StatPearls Publishing.

[2] Vigil, P., Meléndez, J., Petkovic, G., Del Río, J.P., 2022. The importance of estradiol for body weight regulation in women. Frontiers in Endocrinology 13, Doi: 10.3389/fendo.2022.951186.

[3] Mahboobifard, F., Pourgholami, M.H., Jorjani, M., Dargahi, L., Amiri, M., Sadeghi, S., et al., 2022. Estrogen as a key regulator of energy homeostasis and metabolic health. Biomedicine & Pharmacotherapy 156: 113808, Doi: 10.1016/j.biopha.2022.113808.

[4] Weidlinger, S., Winterberger, K., Pape, J., Weidlinger, M., Janka, H., von Wolff, M., et al., 2023. Impact of estrogens on resting energy expenditure: A systematic review. Obesity Reviews: An Official Journal of the International Association for the Study of Obesity 24(10): e13605, Doi: 10.1111/obr.13605.

[5] Rehman, A., Lathief, S., Charoenngam, N., Pal, L., 2024. Aging and Adiposity—Focus on Biological Females at Midlife and Beyond. International Journal of Molecular Sciences 25(5): 2972, Doi: 10.3390/ijms25052972.

[6] Lovejoy, J.C., Champagne, C.M., de Jonge, L., Xie, H., Smith, S.R., 2008. Increased visceral fat and decreased energy expenditure during the menopausal transition. International Journal of Obesity (2005) 32(6): 949–58, Doi: 10.1038/ijo.2008.25.

[7] Duval, K., Prud'homme, D., Rabasa-Lhoret, R., Strychar, I., Brochu, M., Lavoie, J.-M., et al., 2013. Effects of the menopausal transition on energy expenditure: a MONET Group Study. European Journal of Clinical Nutrition 67(4): 407–11, Doi: 10.1038/ejcn.2013.33.

[8] Ward, E., Gold, E.B., Johnson, W.O., Ding, F., Chang, P.-Y., Song, P., et al., 2019. Patterns of Cardiometabolic Health as Midlife Women Transition to Menopause: A Prospective Multiethnic Study. The Journal of Clinical Endocrinology & Metabolism 104(5): 1404–12, Doi: 10.1210/jc.2018-00941.

[9] Ou, Y.-J., Lee, J.-I., Huang, S.-P., Chen, S.-C., Geng, J.-H., Su, C.-H., 2023. Association between Menopause, Postmenopausal Hormone Therapy and Metabolic Syndrome. Journal of Clinical Medicine 12(13): 4435, Doi: 10.3390/jcm12134435.

[10] Xu, Y., Nedungadi, T.P., Zhu, L., Sobhani, N., Irani, B.G., Davis, K.E., et al., 2011. Distinct hypothalamic neurons mediate estrogenic effects on energy homeostasis and reproduction. Cell Metabolism 14(4): 453–65, Doi: 10.1016/j.cmet.2011.08.009.

[11] Correa, S.M., Newstrom, D.W., Warne, J.P., Flandin, P., Cheung, C.C., Lin-Moore, A.T., et al., 2015. An estrogen-responsive module in the ventromedial hypothalamus selectively drives sex-specific activity in females. Cell Reports 10(1): 62–74, Doi: 10.1016/j.celrep.2014.12.011.

[12] van Veen, J.E., Kammel, L.G., Bunda, P.C., Shum, M., Reid, M.S., Massa, M.G., et al., 2020. Hypothalamic estrogen receptor alpha establishes a sexually dimorphic regulatory node of energy expenditure. Nature Metabolism 2(4): 351–63, Doi: 10.1038/s42255-020-0189-6.

[13] Zhang, Z., Reis, F.M.C.V., He, Y., Park, J.W., DiVittorio, J.R., Sivakumar, N., et al., 2020. Estrogen-sensitive medial preoptic area neurons coordinate torpor in mice. Nature Communications 11(1): 6378, Doi: 10.1038/s41467-020-20050-1.

[14] Krause, W.C., Rodriguez, R., Gegenhuber, B., Matharu, N., Rodriguez, A.N., Padilla-Roger, A.M., et al., 2021. Oestrogen engages brain MC4R signalling to drive physical activity in female mice. Nature 599(7883): 131–5, Doi: 10.1038/s41586-021-04010-3.

[15] Rogers, N.H., Perfield, J.W., Strissel, K.J., Obin, M.S., Greenberg, A.S., 2009. Reduced energy expenditure and increased inflammation are early events in the development of ovariectomy-induced obesity. Endocrinology 150(5): 2161–8, Doi: 10.1210/en.2008-1405.

[16] Camporez, J.P.G., Jornayvaz, F.R., Lee, H.-Y., Kanda, S., Guigni, B.A., Kahn, M., et al., 2013. Cellular Mechanism by Which Estradiol Protects Female Ovariectomized Mice From High-Fat Diet-Induced Hepatic and Muscle Insulin Resistance. Endocrinology 154(3): 1021–8, Doi: 10.1210/en.2012-1989.

[17] Musatov, S., Chen, W., Pfaff, D.W., Kaplitt, M.G., Ogawa, S., 2006. RNAi-mediated silencing of estrogen receptor α in the ventromedial nucleus of hypothalamus abolishes female sexual behaviors. Proceedings of the National Academy of Sciences 103(27): 10456–60, Doi: 10.1073/pnas.0603045103.

[18] Sano, K., Tsuda, M.C., Musatov, S., Sakamoto, T., Ogawa, S., 2013. Differential effects of site-specific knockdown of estrogen receptor α in the medial amygdala, medial pre-optic area, and ventromedial nucleus of the hypothalamus on sexual and aggressive behavior of male mice. European Journal of Neuroscience 37(8): 1308–19, Doi: 10.1111/ejn.12131.

[19] Frazao, R., Lemko, H.M.D., da Silva, R.P., Ratra, D.V., Lee, C.E., Williams, K.W., et al., 2014. Estradiol modulates Kiss1 neuronal response to ghrelin. American Journal of Physiology - Endocrinology and Metabolism 306(6): E606–14, Doi: 10.1152/ajpendo.00211.2013.

[20] Qiu, J., Zhang, C., Borgquist, A., Nestor, C.C., Smith, A.W., Bosch, M.A., et al., 2014. Insulin excites anorexigenic proopiomelanocortin neurons via activation of canonical transient receptor potential channels. Cell Metabolism 19(4): 682–93, Doi: 10.1016/j.cmet.2014.03.004.

[21] Padilla, S.L., Perez, J.G., Ben-Hamo, M., Johnson, C.W., Sanchez, R.E.A., Bussi, I.L., et al., 2019. Kisspeptin Neurons in the Arcuate Nucleus of the Hypothalamus Orchestrate Circadian Rhythms and Metabolism. Current Biology: CB 29(4): 592-604.e4, Doi: 10.1016/j.cub.2019.01.022.

[22] Rønnekleiv, O.K., Qiu, J., Kelly, M.J., 2019. Arcuate Kisspeptin Neurons Coordinate Reproductive Activities with Metabolism. Seminars in Reproductive Medicine 37(3): 131–40, Doi: 10.1055/s-0039-3400251.

[23] Hashikawa, K., Hashikawa, Y., Tremblay, R., Zhang, J., Feng, J.E., Sabol, A., et al., 2017. Esr1+ cells in the ventromedial hypothalamus control female aggression. Nature Neuroscience 20(11): 1580–90, Doi: 10.1038/nn.4644.

[24] Lo, L., Yao, S., Kim, D.-W., Cetin, A., Harris, J., Zeng, H., et al., 2019. Connectional architecture of a mouse hypothalamic circuit node controlling social behavior. Proceedings of the National Academy of Sciences 116(15): 7503–12, Doi: 10.1073/pnas.1817503116.

[25] He, Y., Xu, P., Wang, C., Xia, Y., Yu, M., Yang, Y., et al., 2020. Estrogen receptor-α expressing neurons in the ventrolateral VMH regulate glucose balance. Nature Communications 11(1): 2165, Doi: 10.1038/s41467-020-15982-7.

[26] Silva, N.L., Boulant, J.A., 1986. Effects of testosterone, estradiol, and temperature on neurons in preoptic tissue slices. The American Journal of Physiology 250(4 Pt 2): R625-632, Doi: 10.1152/ajpregu.1986.250.4.R625.

[27] Song, Z., Levin, B.E., McArdle, J.J., Bakhos, N., Routh, V.H., 2001. Convergence of pre- and postsynaptic influences on glucosensing neurons in the ventromedial hypothalamic nucleus. Diabetes 50(12): 2673–81, Doi: 10.2337/diabetes.50.12.2673.

[28] Ohki, R., Nemoto, J., Murasawa, H., Oda, E., Inazawa, J., Tanaka, N., et al., 2000. Reprimo, a new candidate mediator of the p53-mediated cell cycle arrest at the G2 phase. The Journal of Biological Chemistry 275(30): 22627–30, Doi: 10.1074/jbc.C000235200.

[29] Xu, M., Knox, A.J., Michaelis, K.A., Kiseljak-Vassiliades, K., Kleinschmidt-DeMasters, B.K., Lillehei, K.O., et al., 2012. Reprimo (RPRM) Is a Novel Tumor Suppressor in Pituitary Tumors and Regulates Survival, Proliferation, and Tumorigenicity. Endocrinology 153(7): 2963–73, Doi: 10.1210/en.2011-2021.

[30] Ye, Z., Wang, J., Shi, W., Zhou, Z., Zhang, Y., Wang, J., et al., 2023. Reprimo (RPRM) as a Potential Preventive and Therapeutic Target for Radiation-Induced Brain Injury via Multiple Mechanisms. International Journal of Molecular Sciences 24(23): 17055, Doi: 10.3390/ijms242317055.

[31] Figueroa, R.J., Carrasco-Avino, G., Wichmann, I.A., Lange, M., Owen, G.I., Siekmann, A.F., et al., 2017. Reprimo tissue-specific expression pattern is conserved between zebrafish and human. PloS One 12(5): e0178274, Doi: 10.1371/journal.pone.0178274.

[32] Nedergaard, J., Cannon, B., 2018. Brown adipose tissue as a heat-producing thermoeffector. Handbook of Clinical Neurology 156: 137–52, Doi: 10.1016/B978-0-444-63912-7.00009-6.

[33] Heine, P.A., Taylor, J.A., Iwamoto, G.A., Lubahn, D.B., Cooke, P.S., 2000. Increased adipose tissue in male and female estrogen receptor-α knockout mice. Proceedings of the National Academy of Sciences 97(23): 12729–34, Doi: 10.1073/pnas.97.23.12729.

[34] Ohlsson, C., Hellberg, N., Parini, P., Vidal, O., Bohlooly-Y, M., Rudling, M., et al., 2000. Obesity and disturbed lipoprotein profile in estrogen receptor-alpha-deficient male mice. Biochemical and Biophysical Research Communications 278(3): 640–5, Doi: 10.1006/bbrc.2000.3827.

[35] Feng, Y., Manka, D., Wagner, K.-U., Khan, S.A., 2007. Estrogen receptor-α expression in the mammary epithelium is required for ductal and alveolar morphogenesis in mice. Proceedings of the National Academy of Sciences of the United States of America 104(37): 14718–23, Doi: 10.1073/pnas.0706933104.

[36] Chow, B.Y., Han, X., Dobry, A.S., Qian, X., Chuong, A.S., Li, M., et al., 2010. High-performance genetically targetable optical neural silencing by light-driven proton pumps. Nature 463(7277): 98–102, Doi: 10.1038/nature08652.

[37] Yang, C.F., Chiang, M.C., Gray, D.C., Prabhakaran, M., Alvarado, M., Juntti, S.A., et al., 2013. Sexually Dimorphic Neurons in the Ventromedial Hypothalamus Govern Mating in Both Sexes and Aggression in Males. Cell 153(4): 896–909, Doi: 10.1016/j.cell.2013.04.017.

[38] Couse, J.F., Lindzey, J., Grandien, K., Gustafsson, J.-Å., Korach, K.S., 1997. Tissue Distribution and Quantitative Analysis of Estrogen Receptor-α (ERα) and Estrogen Receptor-β (ERβ) Messenger Ribonucleic Acid in the Wild-Type and ERα-Knockout Mouse. Endocrinology 138(11): 4613–21, Doi: 10.1210/endo.138.11.5496.

[39] Le May, C., Chu, K., Hu, M., Ortega, C.S., Simpson, E.R., Korach, K.S., et al., 2006. Estrogens protect pancreatic β-cells from apoptosis and prevent insulin-deficient diabetes mellitus in mice. Proceedings of the National Academy of Sciences 103(24): 9232–7, Doi: 10.1073/pnas.0602956103.

[40] Sanchez-Alavez, M., Alboni, S., Conti, B., 2011. Sex- and age-specific differences in core body temperature of C57Bl/6 mice. Age (Dordrecht, Netherlands) 33(1): 89–99, Doi: 10.1007/s11357-010-9164-6.

[41] Krajewski-Hall, S.J., Blackmore, E.M., McMinn, J.R., Rance, N.E., 2018. Estradiol alters body temperature regulation in the female mouse. Temperature (Austin, Tex.) 5(1): 56–69, Doi: 10.1080/23328940.2017.1384090.

[42] Frank, A., Brown, L.M., Clegg, D.J., 2014. The role of hypothalamic estrogen receptors in metabolic regulation. Frontiers in Neuroendocrinology 35(4): 550–7, Doi: 10.1016/j.yfrne.2014.05.002.

[43] Ingberg, E., Theodorsson, A., Theodorsson, E., Strom, J.O., 2012. Methods for long-term 17β-estradiol administration to mice. General and Comparative Endocrinology 175(1): 188–93, Doi: 10.1016/j.ygcen.2011.11.014.

[44] Rubanyi, G.M., Kauser, K., Johns, A., 2002. Role of estrogen receptors in the vascular system. Vascular Pharmacology 38(2): 81–8, Doi: 10.1016/S0306-3623(02)00130-1.

[45] Gieske, M.C., Kim, H.J., Legan, S.J., Koo, Y., Krust, A., Chambon, P., et al., 2007. Pituitary Gonadotroph Estrogen Receptor-α Is Necessary for Fertility in Females. Endocrinology 149(1): 20, Doi: 10.1210/en.2007-1084.

[46] Nadal, A., Alonso-Magdalena, P., Soriano, S., Quesada, I., Ropero, A.B., 2009. The pancreatic beta-cell as a target of estrogens and xenoestrogens: Implications for blood glucose homeostasis and diabetes. Molecular and Cellular Endocrinology 304(1–2): 63–8, Doi: 10.1016/j.mce.2009.02.016.

[47] Hirschberg, P.R., Sarkar, P., Teegala, S.B., Routh, V.H., 2020. Ventromedial hypothalamus glucose-inhibited neurones: A role in glucose and energy homeostasis? Journal of Neuroendocrinology 32(1): e12773, Doi: 10.1111/jne.12773.

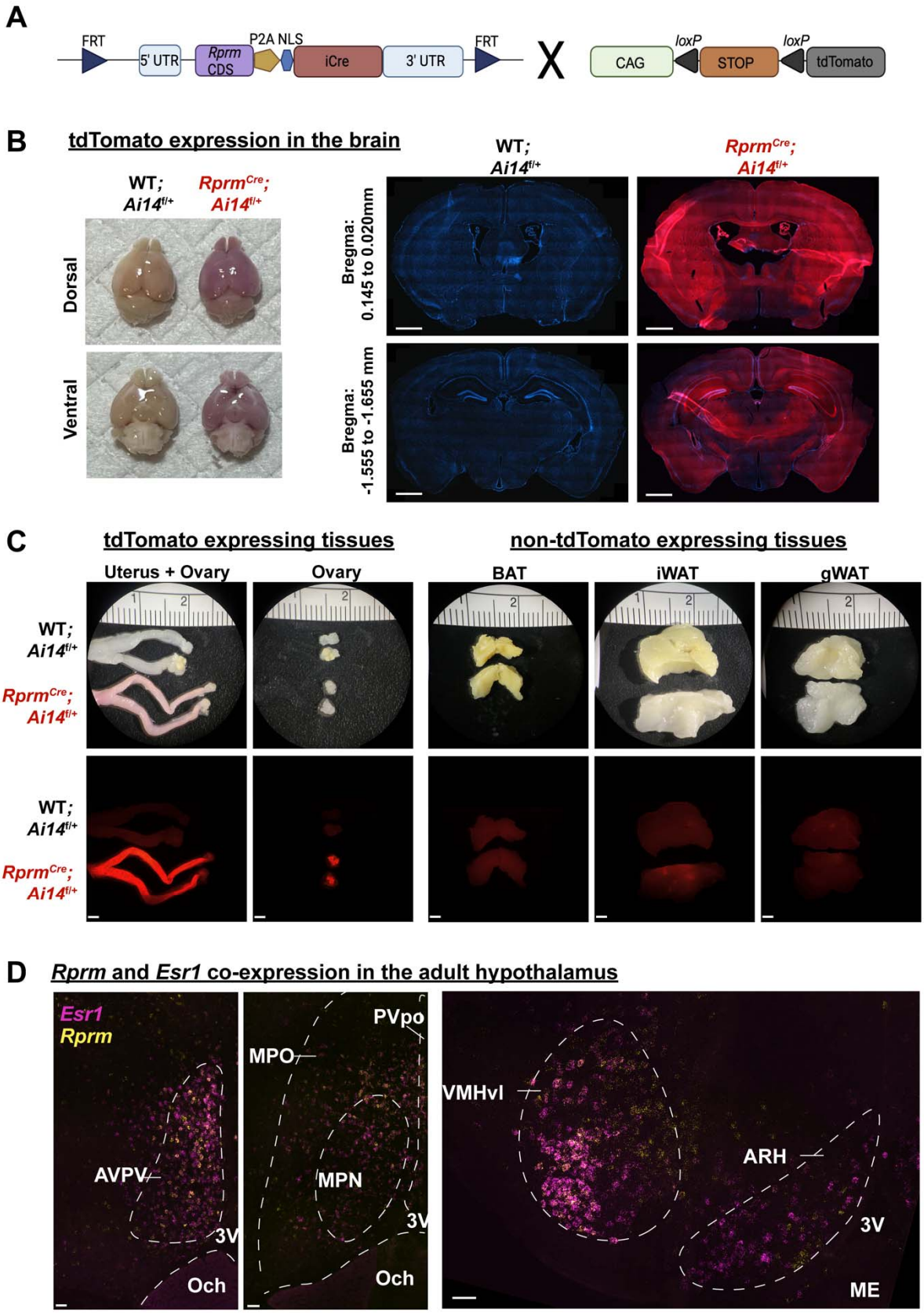

Figure 1: *Rprm* lineage tracing reveals robust expression in the brain and peripheral tissues. (A) Schematic representation for the generation of *Rprm*^{Cre};*Ai14*$^{f/+}$ mice. Heterozygous *Rprm*^{Cre} mice were bred with *Ai14*$^{f/f}$ mice to produce *Rprm*^{Cre};*Ai14*$^{f/+}$ mice expressing tdTomato in *Rprm* lineage tissues. Cre-negative littermates (WT;*Ai14*$^{f/+}$ *mice*) were used to establish baseline tdTomato levels. (B-D) Representative images of tissues harvested from adult (13-15 weeks old) *Rprm*^{Cre};*Ai14*$^{f/+}$ and WT;*Ai14*$^{f/+}$ mice. (B) Left – images highlighting tdTomato expression throughout the whole brain in male mice. Right – 30 µm DAPI-stained coronal brain sections emphasize the expression of tdTomato in the cortex, thalamus, and hypothalamus across representative bregma levels. Scale bars = 1 mm. (C) Left – peripheral tissues exhibiting tdTomato expression include the uterus, & ovary in female mice. Right – adipose tissue depots (BAT, iWAT, and gWAT) do not express tdTomato. Brightfield images displayed on top, fluorescent images below. Scale bars = 200 µm. (D) Single-molecule *in situ* hybridization reveals *Esr1* (magenta) and *Rprm* (yellow) co-expression in the AVPV, VMHvl, and ARH of an adult female mouse and the MPO of an adult male mouse. Dashed lines indicate regions of interest and landmarks. Scale bars = 50 µm. BAT = brown adipose tissue, iWAT = inguinal white adipose tissue, gWAT = gonadal white adipose tissue, AVPV = anteroventral periventricular nucleus, Och = optic chiasm, 3V = third ventricle, MPO = medial preoptic area, MPN = medial preoptic nucleus, PVpo = Periventricular hypothalamic nucleus, VMHvl = ventrolateral area of ventromedial hypothalamus, ARH = arcuate nucleus, ME = median eminence.

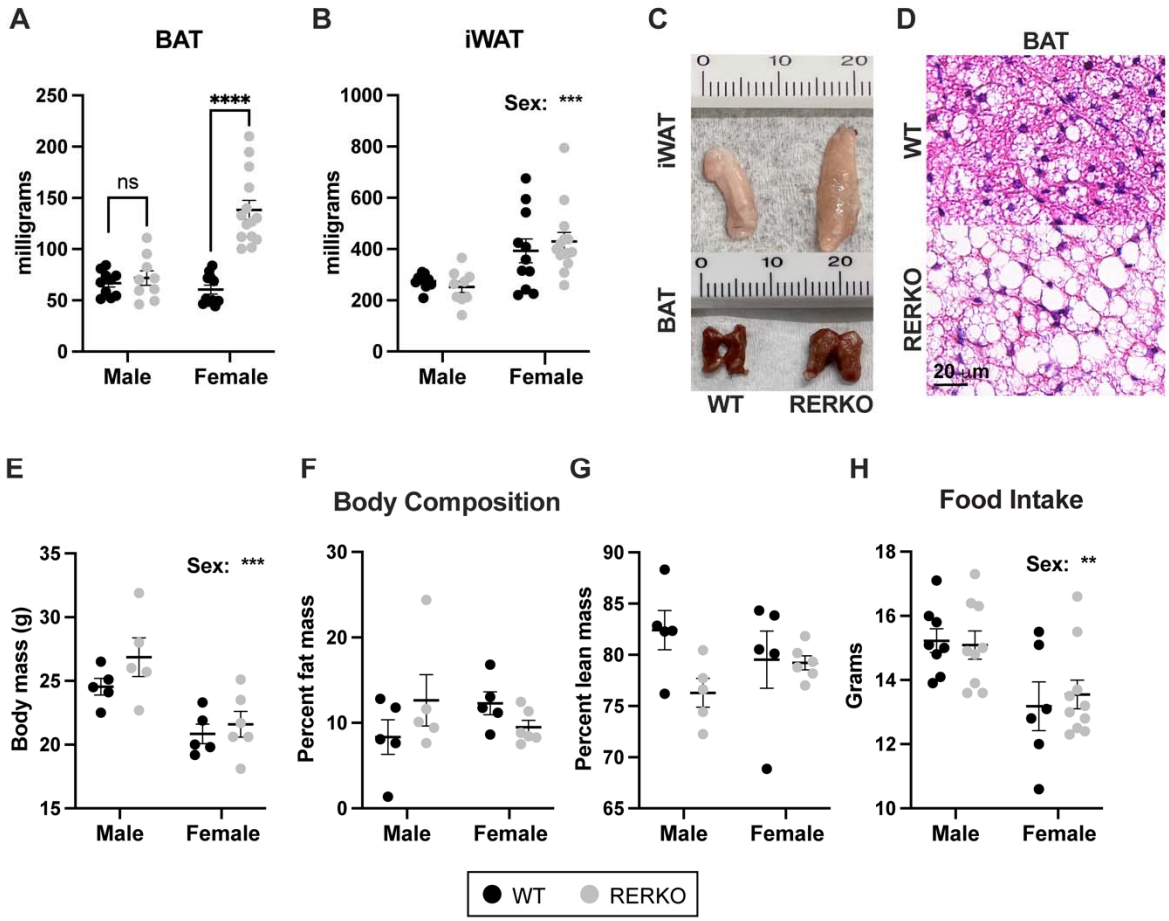

Figure 2. *Esr1* KO in *Rprm* lineage cells (RERKO) sex-specifically alters brown adipose tissue. (A,B) BAT (A) and iWAT (B) mass from adult male and female control littermates (black dots) and RERKO mice (gray dots). N = 10 WT males, 11 WT females, 9 RERKO males, and 14 RERKO females. (C) Representative images of iWAT (top) and BAT (bottom) in WT (left) and RERKO (right) mice. Ruler with centimeters added for scale. (D) Representative images of hematoxylin and eosin staining of WT (top) and RERKO (bottom) in 8-week-old mice. Scale = 20 μm. (E-G) Body composition analysis of male and female WT and RERKO mice at 16 weeks of age via EchoMRI: body mass (E), percent fat mass (F), and percent lean mass (G). N = 5 WT males, 5 WT females, 5 RERKO males, and 6 RERKO females. H) Food consumption averaged over seven days in WT and RERKO mice. N = 8 WT males, 6 WT females, 9 RERKO males, and 10 RERKO females. The mean and standard error of the mean are depicted on all graphs, as well as individual data points. Two-way ANOVAs used for statistical analysis; differences between WT and RERKO tested within each sex using Šídák's multiple comparisons test following a significant interaction. ** $p < .01$, *** $p < 0.001$, **** $p < 0.0001$.

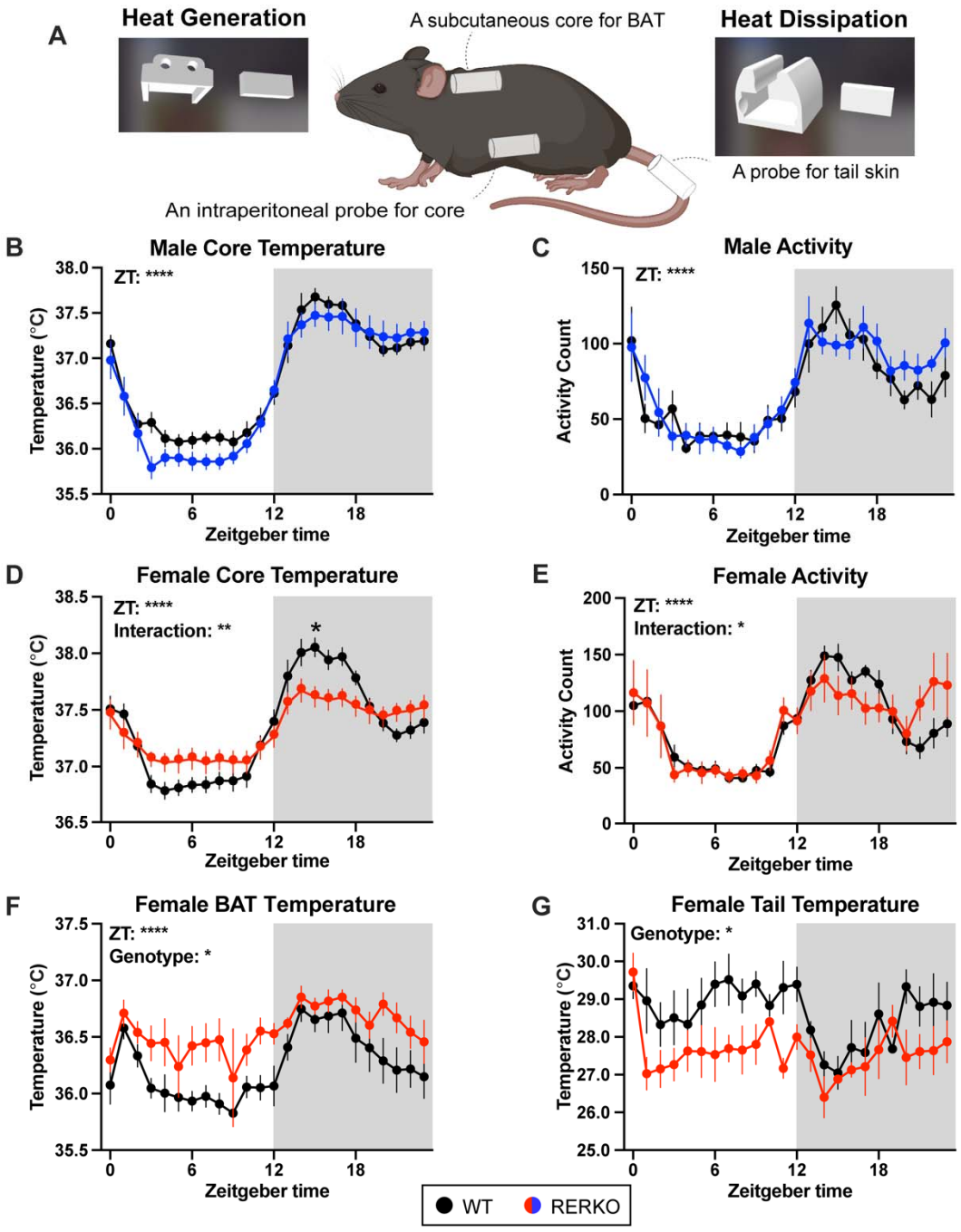

Figure 3. KO of *Esr1* in *Rprm* lineage cells sex-specifically impacts thermoregulation.
(A) Illustration of a mouse implanted with an intraperitoneal probe to record temperature and locomotion. In addition, a probe is placed above the BAT and on the base of the tail to measure heat generation and heat dissipation, respectively. Custom 3d printed sleeves are used to secure the probes. (B-E) Core body temperature in Celsius or activity counts of WT siblings (black) and RERKO mice (males in blue; females in red) averaged hourly across 24 hours. N = 8 WT males, 8 RERKO males, 11 WT females, 10 RERKO females. (F, G) Temperature averaged hourly above the BAT or at base of the tail in female control (black) and RERKO (red) across 24 hours.

N for BAT data = 8 WT, 8 RERKO. N for tail data = 4 WT, 4 RERKO. Mean and standard error of the mean plotted at each time point. Two-way mixed ANOVAs used for statistical analyses. Significant interaction followed by Šídák's multiple comparisons at each time point. ZT = Zeitgeber time. C = Celsius. Shaded box indicates the dark (active) phase of the day.

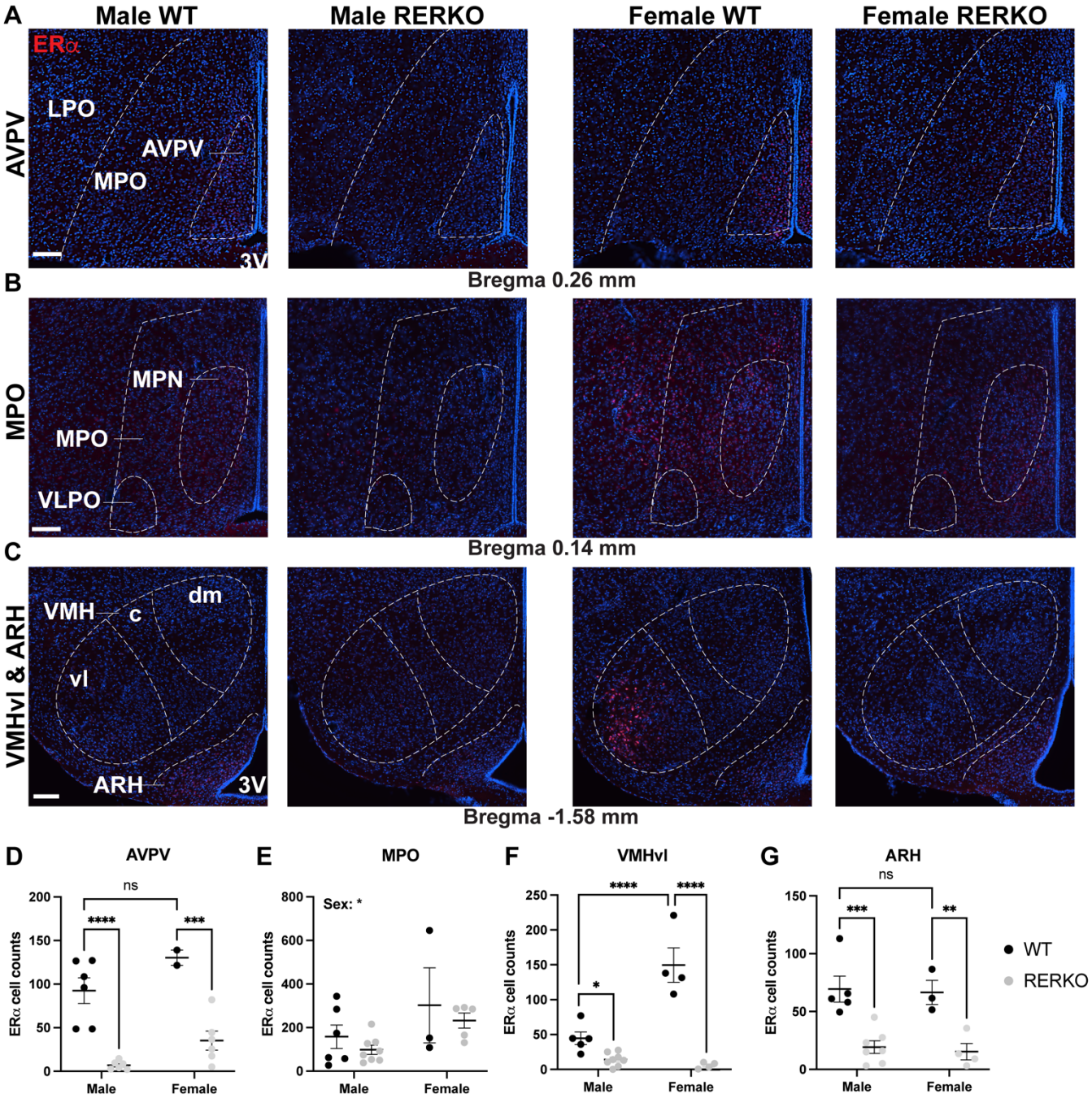

Figure 4. RERKO mice have reduced ERα immunoreactivity in hypothalamic thermoregulatory hubs. (A-C) Images of ERα immunoreactivity (red) in coronal sections of the brain containing the anteroventral periventricular area (A; AVPV), medial preoptic area (B; MPO), ventrolateral area of the ventromedial hypothalamus (C; VMHvl), and arcuate nucleus (C; ARH). Tissue is counterstained with DAPI (blue). (D-G) Quantification of ERα+ cells in male and female WT (black dots) and RERKO (gray dots) mice in the AVPV (D), MPO (E), VMHvl (F) and ARH (G) (N = 2 - 8 per group). Statistical analysis performed using Two-way ANOVA followed by Šídák's multiple comparisons test, if applicable. The mean and standard error of the mean are depicted. Individual data points are shown in figures. ** $p < .01$, *** $p < 0.001$, **** $p < 0.0001$. Scale bars = 100 μm. Boundaries of nuclei and landmarks outlined to aid

in visualization. LPO = lateral preoptic area, MPN = medial preoptic nucleus, VLPO = ventrolateral preoptic area. dm = dorsomedial, c = caudal, 3V = third ventricle.

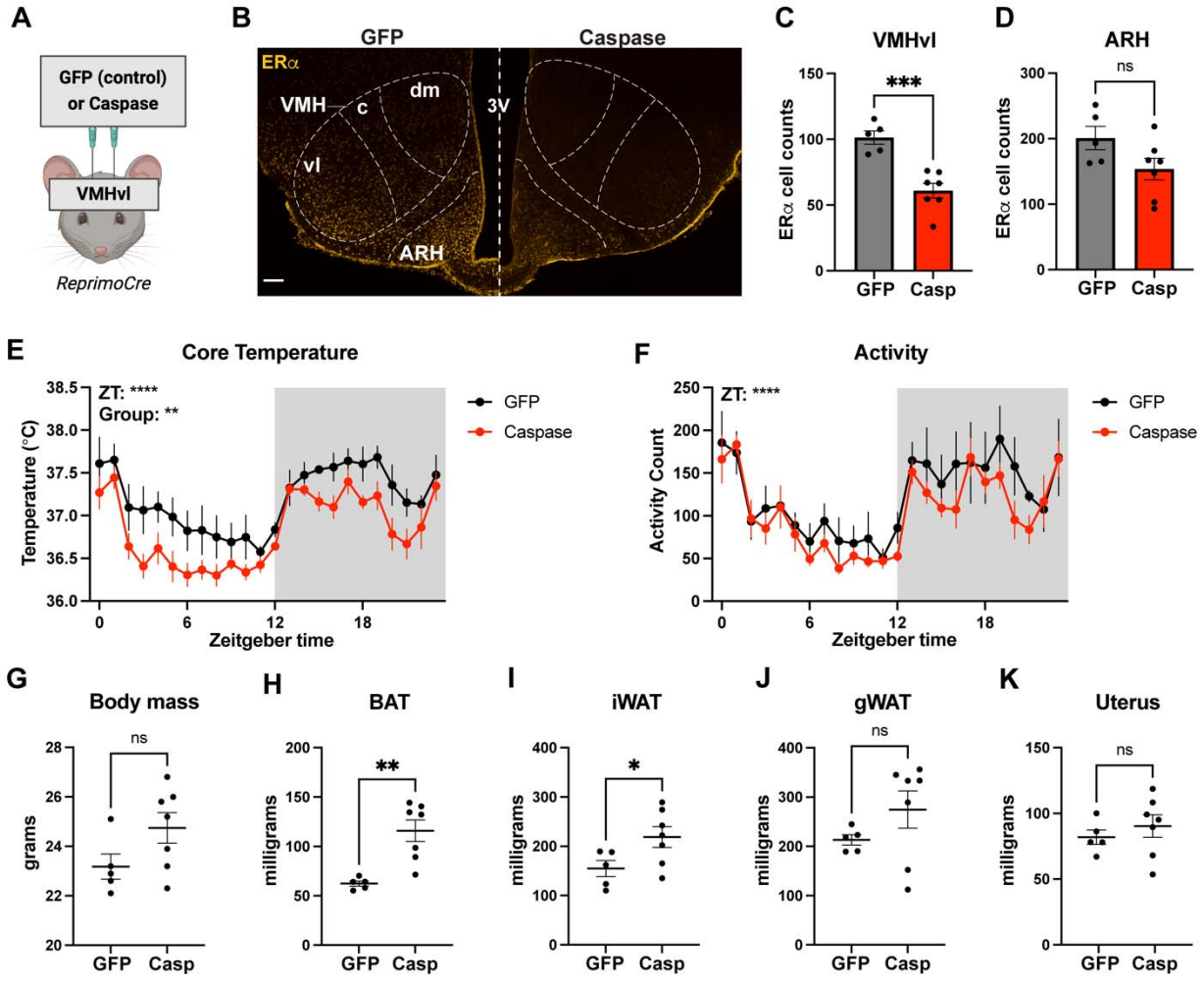

Figure 5. Ablating *Reprimo*+ cells in the ventromedial hypothalamus (VMH) reduces core temperature in female mice. (A) Illustration depicting the stereotaxic delivery of a cre-dependent caspase or control virus into the VMHvl of female mice. (B) Image of ERα immunoreactivity (yellow) in the mediobasal hypothalamus in a control (GFP; left) and caspase-treated (casp; right) mouse. Nuclei delineated to aid in visualization. (C, D) Quantification of ERα+ cells in the VMHvl and ARC in control (gray bar) and caspase-treated (red bar) female mice. (E, F) Core temperature and activity counts averaged hourly across 24 hours in control (black) and caspase-treated (red) mice. (G) Body mass of control (GFP) and caspase-treated mice at 8 weeks of age. (H-K) Mass of dissected BAT (H), iWAT (I), gonadal WAT (J), and uterus (K) from GFP and caspase mice. N = 5 GFP and N = 7 caspase for all plots. Statistical analysis performed using t-test or mixed model Two-way ANOVAs. The mean and standard error of the mean are depicted. Individual data points are shown in figures C-D and G-K.* $p < 0.05$, ** $p <$ .01, **** $p < 0.0001$. Scale bar = 100 μm. VMH = ventromedial hypothalamus (c = caudal, dm = dorsomedial, and vl = ventrolateral areas), ARH = arcuate nucleus, 3V = third ventricle.

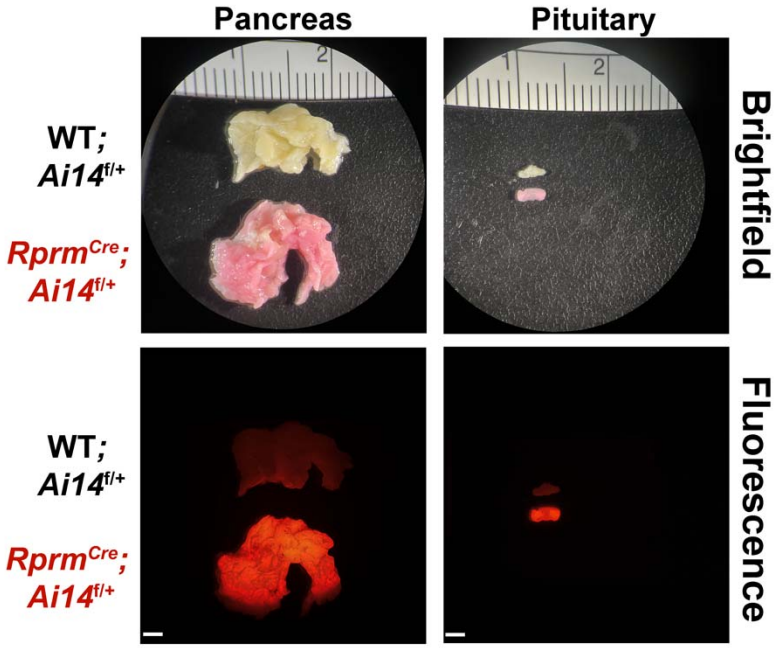

Supplementary Figure 1: Additional tissues displaying tdTomato expression in *Rprm^{Cre};Ai14$^{f/+}$* mice. Tissue harvesting and imaging reveal the expression of tdTomato in the pancreas and pituitary in female mice. Brightfield images displayed on top, fluorescent images below. Scale bars = 200 μm.

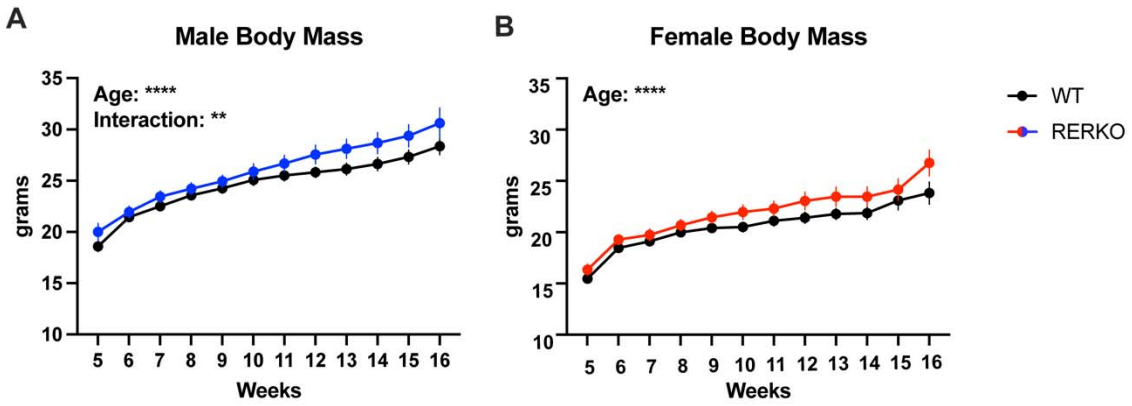

Supplementary Figure 2. Longitudinal body weight analysis of RERKO mice. (A) Body mass measurements of control (black) and RERKO (blue) male mice from 5 to 16 weeks of age (n = 16 WT, n = 18 RERKO). (B) Body mass measurements of control (black) and RERKO (red) female mice from 5 to 16 weeks of age (n = 13 WT, n = 13 RERKO). In females, we only detected an effect of age ($F_{11,238} = 61$, $p < 0.0001$). Mean and standard error of the mean plotted at each time point. A mixed-effects model using Restricted Maximum Likelihood (REML) estimation was used for statistical analysis due to missing values.

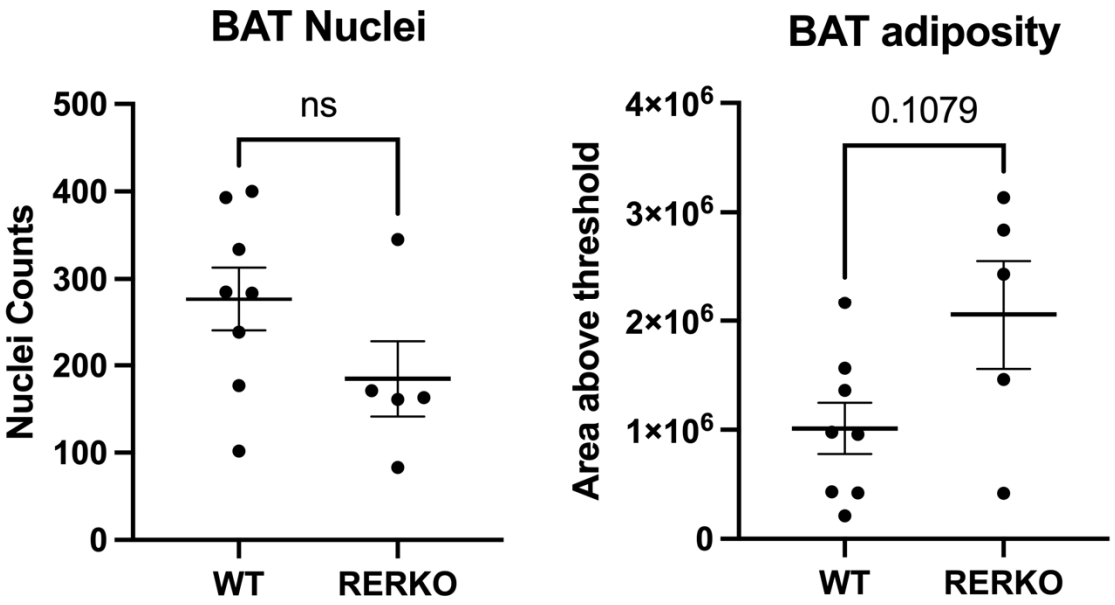

Supplementary Figure 3. BAT nuclei and BAT adipose quantification in control and RERKO mice. A) Nuclei within a fixed area of BAT tissue were counted in 40x images in control and RERKO adult female mice. B) To roughly compare the adiposity in BAT tissue, the total area of the white portion of BAT images (a proxy for fat droplets) was also estimated using thresholding analysis in ImageJ. Statistical analysis performed using t-test.

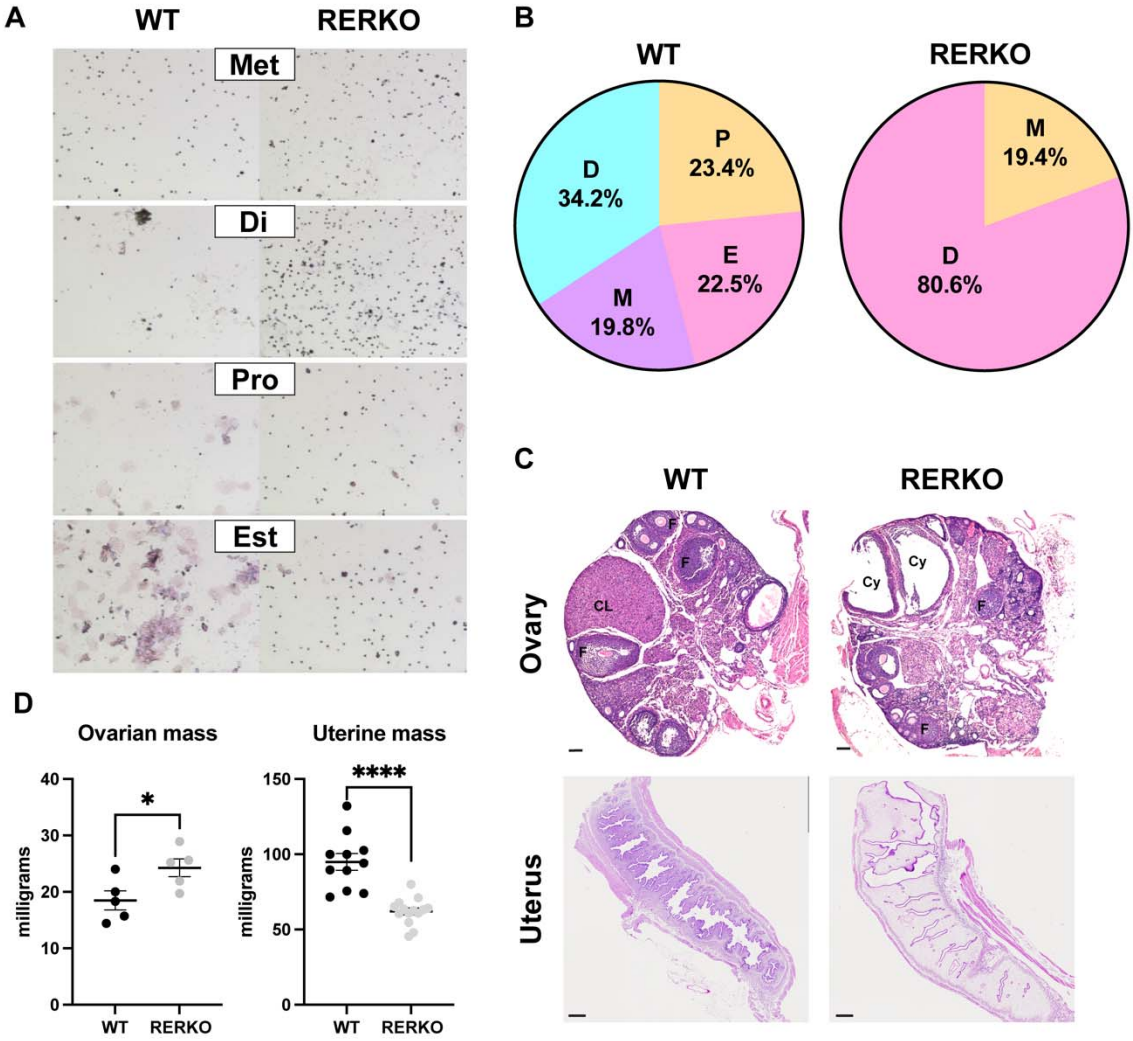

Supplementary Figure 4. RERKO female mice have disrupted reproduction. (A) Images depict vaginal lavages from WT (left) and RERKO (right) mice stained with Giemsa. While the WT mice display expected cellular morphological changes across the estrous cycle, swabs from RERKO mice mostly contain leukocytes. (B) The percent of days across 14 days spent in diestrus [D], proestrus [P], estrus [E], and metestrus [M] in WT (left) and RERKO (right) mice. (C) Ovarian histology visualized with hematoxylin & eosin stain. Follicular cysts are present and the corpus luteum is absent in the ovary from RERKO mice. CL = corpus luteum, F = ovarian follicles, Cy = cyst. Scales are 100 µm (ovary) and 500 µm (uterus). D) Dissected ovarian and uterine mass from control (black) and RERKO (gray) mice. T-test used to compare between groups. The mean and standard error of the mean are depicted. Individual data points are shown in Figure D. * $p < 0.05$, **** $p < 0.0001$.

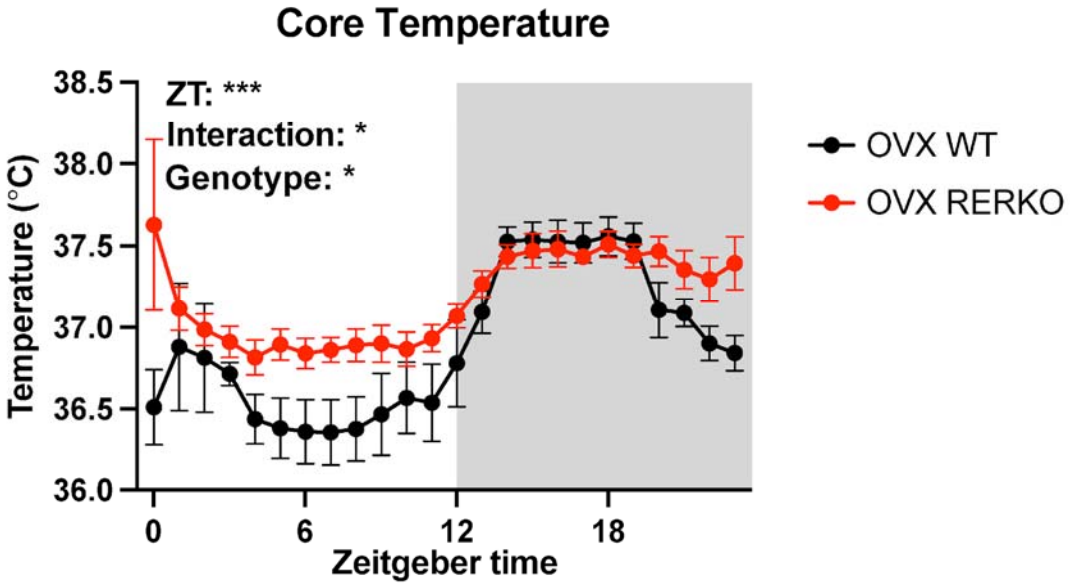

Supplementary Figure 5. Core temperature in RERKO mice lacking ovaries. Core temperature averaged hourly across 24 hours in ovariectomized (OVX) WT littermates (black) or RERKO (red) mice. Two-way mixed ANOVAs used for statistical analysis. The mean and standard error of the mean are depicted for each hour. * $p < 0.05$. ZT = Zeitgeber time. C = Celsius. Shaded box indicates the dark (active) phase of the day.